UV-Induced Nonlinear Absorption in Lanthanum Calcium Borate Single Crystals

I. V. Kityk,*,† A. Majchrowski,‡ E. Michalski,‡ D. Kasprowicz,§ M. Drozdowski,§ J. Kisielewski,|| T. Lukasiewicz,|| and B. Sahraoui⊥

Institute of Physics, J. Dlugosz Academy of Czestochowa, Al. Armii Krajowej 13/15, Czestochowa, Poland, Institute of Applied Physics, Military University of Technology, 2 Kaliskiego Str., 00-908 Warsaw, Poland, Faculty of Technical Physics, Poznan University of Technology, Nieszawska 13 A, 60-965 Poznan, Poland, Institute of Electronic Materials Technology, 133 Wolczanska Str., 01-919 Warsaw, Poland, and Laboratoire POMA, UMR CNRS 6136, Universite d'Angers, Angers, France

Received: January 5, 2006; In Final Form: March 16, 2006

It has been revealed that lanthanum calcium borate ($La_2CaB_{10}O_{19}$) crystals show two-photon absorption (TPA) induced by a UV laser field. UV-induced TPA measurements were performed in the spectral range of 475−1130 nm using as fundamental beam the third harmonics of the 28 ps Nd−YAG pulsed laser as a pumping beam for LiB_3O_5 optical parametrized generator using Z-scan method. Investigations performed by the *Z*-scan method were done during illumination by a Xe−F laser ($\lambda = 217$ nm) as a photoinducing (pumping) beam. The pumping laser beam created a thin surface layer (about 80−90 nm) that was the source of the observed photoinduced TPA. The highest values of the TPA β coefficients were achieved for polarization of the pumping light directed along the second-order crystallographic axis of the investigated crystals. The obtained values of the TPA coefficients were higher than those for the BiB_3O_6 crystals investigated earlier by us.

1. Introduction

Due to possible 3- or 4-fold coordination of boron atoms, borates form a great number of compounds possessing diverse structures. Many of them show superior nonlinear optical properties compared to well-known inorganic compounds.[1] These single-crystalline borates find numerous applications in laser and nonlinear optics (NLO). Especially, borate crystals play important roles in UV applications due to their relatively high UV transparency, good NLO efficiency, and high damage threshold for laser radiation. The borate crystals have been widely studied in the last several years, and as a result several new promising materials such as $CsLiB_6O_{10}$ (CLBO),[2] $Ca_4ReO(BO_3)_3$, Re = Gd, Y (ReCOB), and BiB_3O_6 (BiBO) have been found.[3−6] These crystals allow efficient generation of radiation in the UV and visible regions due to the higher harmonics generation of external laser medium sources or self-frequency doubling (SFD) when a crystal acts simultaneously as a laser and NLO material. One of the possible borate crystals showing NLO properties is lanthanum calcium borate $La_2CaB_{10}O_{19}$ (LCB) discovered by Wu et al.[7] The material crystallizes in an acentric structure (monoclinic, space group *C*2). It has slightly higher birefringence than YCOB (0.053 and 0.041 at 1064 nm, respectively), which allows second harmonic generation (SHG) in this material down to 288 nm, compared to 360 nm for YCOB.[8] La^{3+} ions in this crystal provide sites for Nd^{3+} [9] or Yb^{3+} [10] substitution. As a result a multifunctional material showing SFD properties may be synthesized. Moreover, according to Wang et al.[11] its effective optical second-order susceptibility d_{eff} (1.05 pm/V, $\lambda = 1.06\ \mu$m) is larger than those for LiB_3O_5 (LBO) and KH_2PO_4 (KDP). Besides, the LCB is insensitive to moisture contrary to LBO, KDP, and β-BaB_2O_4 (BBO), and the damage threshold is higher than that of BBO and $KTiOPO_4$ (KTP). All of these features make LCB crystals a good candidate for SHG conversion applications. In this paper we describe investigations of UV-induced two-photon absorption in LCB crystals.

2. $La_2CaB_{10}O_{19}$ Crystal Growth

According to the phase diagram given by Wu et al.[8] LCB melts incongruently. As a consequence high-temperature solution growth should be used to obtain a single-crystalline form. According to Wang et al.[12] Czochralski growth of LCB crystals from stoichiometric melts is also possible due to a small difference in melting temperature and the peritectic phase transition temperature of the LCB. However such a crystallization is disturbed by crystallization of lanthanum borate LaB_3O_6 at the bottom of the crucible. The phase diagram of the system LaB_3O_6−CaB_4O_7 shows that over a broad range of composition, when an excess of CaB_4O_7 is used, the monoclinic LCB phase is the only crystallizing phase.[8]

In our technology an excess of CaB_4O_7 was used as a solvent. The synthesis of the starting material was carried out under strict control to avoid changes in composition of the melt caused by evaporation of CaB_4O_7. Wu et al.[8] carried out the LCB crystallization from melts containing 30 mol % excess of calcium tetraborate compared to the stoichiometric composition. Our investigations suggest that 30 mol % excess of CaB_4O_7 may be not sufficient because of strong evaporation of the solvent that could shift the composition of the melt to the area of LaB_3O_6 crystallization. We used nearly 60 mol % of CaB_4O_7 in the LaB_3O_6−CaB_4O_7 system given in ref 8. A two-zone resistance furnace was used to crystallize LCB from a platinum crucible. The lower zone secured the proper temperature of the

* Author to whom correspondence should be addressed. Phone: (48) 601 50 42 68. E-mail: i.kityk@ajd.czest.pl.
† J. Dlugosz Academy of Czestochowa.
‡ Military University of Technology.
§ Poznan University of Technology.
|| Institute of Electronic Materials Technology.
⊥ Universite d'Angers.

10.1021/jp060079f CCC: $33.50
Published on Web 04/20/2006

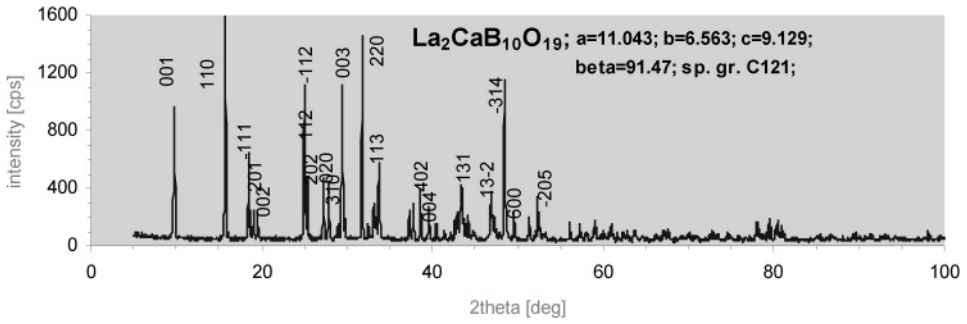

Figure 1. X-ray powder diffraction pattern of LCB crystals.

melt, while the upper zone was used to diminish the temperature gradients in the crystallization region, which is a necessary condition during high-temperature solution growth. The details of the crystallization set can be found elsewhere.[13] Recrystallized rods of LCB glass were used as seeds during processes of top seeded solution growth (TSSG). Due to the polycrystalline structure of these seeds LCB crystallized in the form of numerous plates having average dimensions of $3 \times 3 \times 1$ mm^3, which were used in our investigations. In Figure 1 we present a powder X-ray diffraction pattern confirming the monoclinic structure of the obtained crystals ($a = 11.043$Å, $b = 6.563$ Å, $c = 9.129$ Å, and $\beta = 91.47°$). The obtained crystals will be used in future experiments as seeds to obtain more bulky LCB single crystals.

3. Third-Order Optical Properties of BiBO

3.1. General Formalism of Two-Photon Absorption. The LCB crystals may be also of interest because of the third-order optical applications, particularly for the two-photon absorption (TPA) described by the imaginary part of fourth-rank optical susceptibility and more generally for nonlinear optical absorption.

Nonlinear optical effects are generally described phenomenologically by the optical response P, of a material to an effective electric field, E[14]

$$P_i(\vec{\mathbf{r}},t) = \chi_{ij}^{(1)} \cdot E_j(\vec{\mathbf{r}},t) + \chi_{ijk}^{(2)} \cdot E_j E_k(\vec{\mathbf{r}},t) + \chi_{ijkl}^{(3)} \cdot E_j E_k E_l(\vec{\mathbf{r}},t) + \cdots \quad (1)$$

The $\chi_{ij}^{(1)}$ term is responsible here for linear optics phenomena such as light reflection and refraction. The terms $\chi_{ijk}^{(2)}$ and $\chi_{ijkl}^{(3)}$ are responsible for nonlinear optical phenomena and correspond to the second- and third-order optical effects, respectively. E_k and E_l are effective electric field strength components determined by electromagnetic wave strengths.

When the charges in a material are bound by a harmonic potential, the induced dipole moment is linear to the applied electric field. The response of a molecule is nonlinear if the charges are bound to the molecule by an anharmonic potential. In this case, the dipole moment of the molecule is a nonlinear function of applied electric field strength. More generally, if a "nonlinear" molecule is exposed to light, then the time-dependent induced dipole moment is a nonlinear function of the time-dependent electric field. For a slowly varying electric field, the induced molecular dipole moment and corresponding polarizability, P, can be expanded as a power series versus the applied electric field E[14]

$$P_i(\vec{\mathbf{r}},t) = P_l^{(0)} + \alpha_{ij} \cdot E_j(\vec{\mathbf{r}},t) + \beta_{ijk} \cdot E_j E_k(\vec{\mathbf{r}},t) + \gamma_{ijkl} \cdot E_j E_k E_l(\vec{\mathbf{r}},t) + \cdots \quad (2)$$

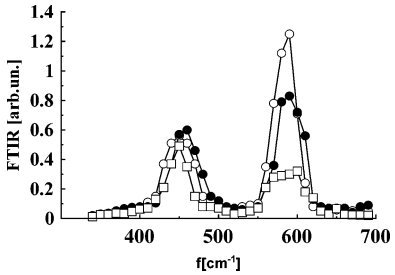

Figure 2. Changes of the FTIR spectra versus different UV-induced power densities: □, 0.1 GW/cm^2; ●, 0.4 GW/cm^2; ○, 0.8 GW/cm^2.

where the subscripts refer to the Cartesian vector or tensor components of each quantity, $P_l^{(0)}$ is the ith component of the crystal's static dipole moment, α_{ij} is the linear microscopic polarizability, and β_{ijk} and γ_{ijk} correspond to first- and second-order susceptibilities, respectively.

Generally the TPA does not require a charge density noncentrosymmetry. However the TPA is determined by dipole moments both of ground as well as of excited states. To create additional possibilities of using materials as third-order media it is necessary to create substantial enhancement of the corresponding dipole moments.

One can clearly see substantial enhancement of the anharmonic phonon modes during increases of the UV-induced power (Figure 2), contrary to the usual harmonic mode observed at about 585 cm^{-1}. The phonon modes situated at lower frequencies (for example, at 450 cm^{-1}) are almost insensitive to UV induction. So this fact indicates the occurrence of photoinduced anharmonic modes within the bulk crystals propagating from the thin UV-induced layers through the crystal. A similar situation was observed in the BiB_3O_6 single crystals.[15]

3.2. *Z*-Scan Measurements. At the moment a more powerful method for determination of the nonlinear absorption and refractive indices is *Z*-scan method. The main principles of the *Z*-scan technique were developed in many works (see, for example, refs 16−17). Basic principle of the method consists in a variation of the effective diameter of fundamental beam on the sample surface. Detection of the optical signal through the sample is done by a detector behind an aperture. Moving the specimen along the beam propagation direction (indicated as *z*-direction) one can measure transmittance versus sample position. The nonlinearities are evaluated from absorption depending on the sample positions. Optical nonlinearities consists of two parts: nonlinear absorption and refraction. Assuming a Gaussian beam profile the nonlinear absorption coefficient β is determined from measurement of the total power densities passing through the sample. Optimal absorption usually occurs when the sample is situated near the focal plane sequence.

So in this case we used an open aperture, which is independent of the nonlinear refraction, and we take into account

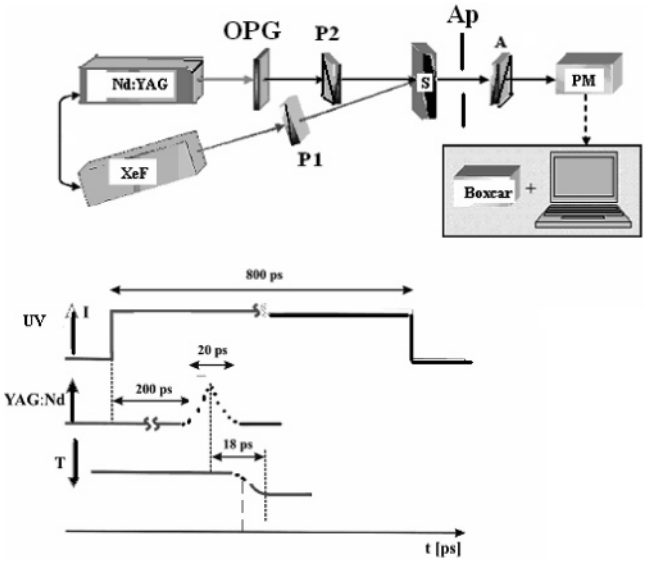

Figure 3. Principal schemes of the experimental setup.

only the nonlinear optical absorption. To evaluate the nonlinear refraction coefficient γ we use the regime of transmittance measurements with a very small, almost closed aperture. In this case we were able to evaluate phase shift directly related with the refractive indices.

Assuming a Gaussian beam profile within a framework of a thin-sample approximation the coefficient of transmittance T may be presented following the formalism developed in ref 18. TPA measurements were performed in the spectral range of 475−1130 nm using as fundamental beam the third harmonics of the 28 ps Nd−YAG pulsed laser as a pumping beam for LiB_3O_5 optical parametrized generator (OPG) by Z-scan method (see Figure 3). The value of the waist radius has been changed within 20−35 μm depending on the wavelengths with a Rayleigh range equal to about 3.2−3.55 μm. As a reference for nonlinear absorption measurements we have used single crystals of ZnS with the known parameters of the two-photon absorption in the investigated spectral range. In the regime of a closed-aperture Z-scan to measure nonlinear refraction the linear transmission of the closed apertures was kept fixed with a value equal to about 0.14. All of the measurements were done with a pulse frequency repetition equal to about 7 Hz. The experiments were performed both during excitation by a UV excimer laser operating at 217 nm as well as without the UV illumination. To eliminate any scattering of the UV-pumped light an additional UV filter was installed. The probe power densities after the optical parametrical generators were varied between 0.015 and 4.2 GW/cm^2.

As a reference, we chose a ZnS plate with known nonlinear absorption and refractive indices. The imaginary part of the third-order optical susceptibility was determined by a method described in the ref 19.

The UV-inducing (pumping) excimer laser with a pulse duration of about 800 ps and a power density of about 1.5 GW/cm^2 was used as a source of the pumping illumination. The LiF polarizer P1 defined the polarization direction of the incident pumping beam. The excimer pumping laser (λ = 217 nm) creates strong electric strength in thin nanolayer of the LCB crystal. Due to large absorption of the crystal at this wavelength it creates a photoinduced layer (about 80−90 nm) with an enhanced number of UV-excited states.

The fundamental power densities have been varied within 0−1.5 GW/cm^2 with an increment equal to about 0.05 GW/cm^2. An angle between directions of propagation of the fundamental and pumping beams was equal to about 12°. The polarizers P1 and P2 were allowed to operate by polarizations of the fundamental and pumping laser beams. The pumping and fundamental laser beams have been temporary synchronized. The precision of determination of the delaying time between the fundamental and the pumping laser beams was equal to about 2−3 ps. The delaying time of about 18 ps was registered by a fast-response photomultiplier connected with the boxcar by the delaying time position of the laser pulse maximums. The precision of the delaying time is determined by statistic averaging over 100−120 pulses. The registration system consisting of a photomultiplier and an electronic boxcar allowed the evaluation of values of transparency with a precision equal to about 2−3%. For convenience the measured points are presented by the labels possessing sizes corresponding to error bars. Typically the delaying time between the end of the pumping beam and the saturation of the photoinduced transparency is equal about 20 ps.

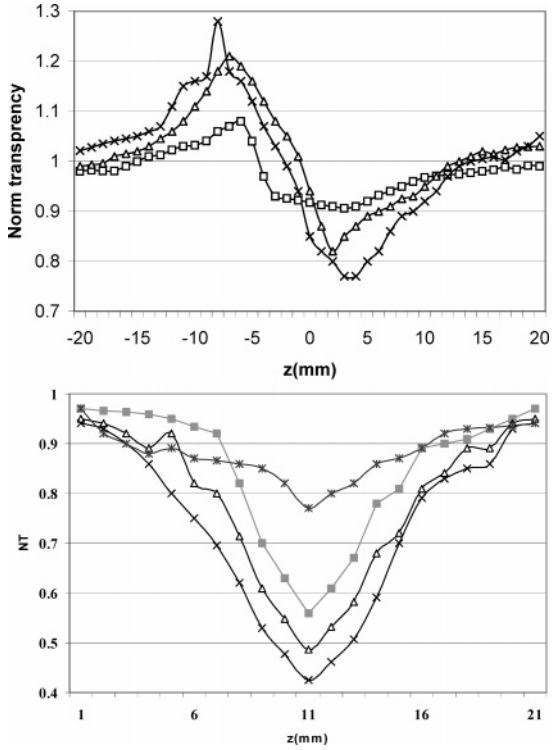

Figure 4. (a) Z-scan with a closed aperture (CA): □, without the UV-induced excitation; △, at a UV excitation power density of 0.5 GW/cm^2; ×, at a UV excitation power density of 0.8 GW/cm^2. (b) Z-scan with an open aperture (OA): ∗, without the UV-induced photoillumination at a fundamental power density of 1 GW/cm^2; □, at a UV-induced excitation power density of 0.5 GW/cm^2; △, at 0.8 GW/cm^2; ×, at 1.1 GW/cm^2.

The registration system consisting of the PM together with the electronic boxcar registration system allows monitoring of the kinetics of the output transparency versus the intensity power of the probing laser beams.

3.3. Results of the Nonlinear Absorption Measurements and Discussion. Typical measured UV-induced intensity-dependent transparencies for the open and closed apertures are shown in Figure 4. From the figures one can see that enhancement of the UV-pumping power densities unambiguously enhances the amplitudes of the Z-scan. This fact explains why the effect is caused by the UV excimer laser beams. Because the UV-pumping beam penetrates only into the thin nanometer

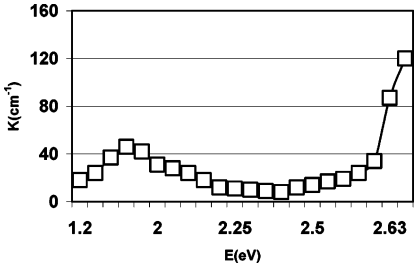

Figure 5. Linear absorption of the LCB.

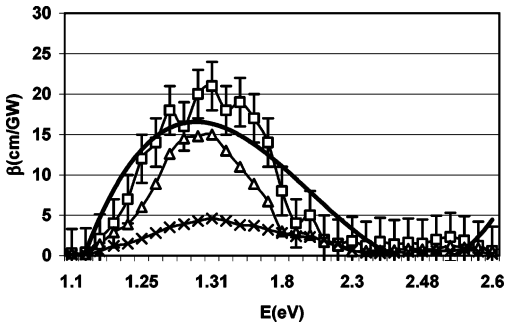

Figure 6. Experimental UV-excited TPA coefficient *b* at different pump powers: △, 0.75 GW/cm^2; □, 1.1 GW/cm^2; ×, without UV excitation. The solid line corresponds to theoretical calculations following band structure calculations at an effective pump power of 1 GW/cm^2.

layers of the investigated crystals one can understand that the only way to enhance the third-order susceptibility determined nonlinear absorption may be due to phonons, which is demonstrated in Figure 2. Assuming the Gaussian beam profile we have evaluated the spectral dependences of the two-photon absorption coefficient. For every wavelength we have done separately the measurements of the *Z*-scan transparency, which allowed us to obtain spectral dependences of the TPA presented in Figure 5. This figure clearly demonstrates enhancement of the TPA due to the UV-induced excitation. It is necessary to emphasize that the linear ion spectra presented in Figure 6 were not sensitive to the UV-inducing illumination. To explain additionally the physical insight of the nonlinear absorption, we have done the band energy structure calculations of the LCB crystals under an applied external electric field corresponding to the pumping power density equal to about 1 GW/cm^2. To perform investigations of the contribution of the two-photon absorption to the observed phenomenon we have done band energy structure calculations. Through the use of these data we have evaluated the parameters of the two-photon susceptibilities under influence of the UV excitations. Density functional theory calculations for the monoclinic semiconducting $La_2CaB_{10}O_{19}$ crystal are shown in the Figure 7. In our calculations we used the first-principles, self-consistent, tight-binding, linear muffin-tin orbital (TB-LMTO) of the Anderson and Jepsen[18] method. The von Barth−Hedin[19] parametrization is used for the exchange correlation. Figure 7 shows the band energy dispersion and the density of states (DOS) of the investigated LCB crystals calculated by using the TB-LMTO as described in ref 20.

From Figure 7 one can see that the valence and conduction bands have substantially different band energy dispersion, which corresponds to substantially different mobilities between the localized holes and delocalized nonoccupied semiconducting bands. Such a situation is extremely important for different kinds of photoinduced effects due to excitation of the localized excitons to the delocalized band states. At the same time the

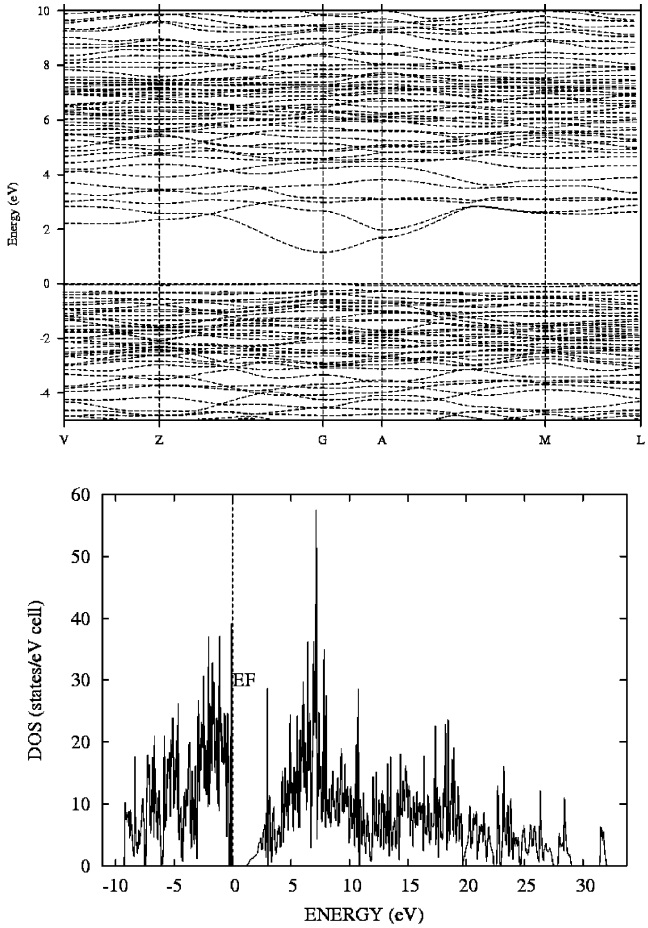

Figure 7. Band structure and DOS for the LCB crystals.

susceptibilities should also be maximal for these bands due to the substantially different values of effective masses within 1.2−6 eV. The more effective pumping may be observed near the G and Z symmetry points of the BZ. We note that the valence band maximum (VBM) is located at Z and the conduction band minimum (CBM) at G, resulting in an indirect energy gap of 1.5 eV.

A similar situation is observed for the DOS, which unambiguously shows that the effect will be maximal for wavelengths of about 215 nm. So we should use those wavelengths for the pumping, and the maximal gradient should be observed at 2.4 eV (619.5 nm), so these wavelengths should be used for the probing beams.

The data obtained were used for evaluations of the TPA. Their efficiency is at least 3 times higher than that in the case of BiBO crystals.[15]

One can see that the figure shows sufficiently good spectral dependence of the UV-induced and theoretically simulated TPA, which may indicate that the higher values of the TPA were achieved for the polarization of the pump light directed along the second-order optical axis, corresponding to the χ_{2222} tensor component. This fact reflects the substantial contribution given by the anharmonic electron−phonon interactions to the TPA. One can expect that the thin UV-induced layer is a source of anharmonic phonons contributing to the observed TPA. Varying the samples' thickness within the 0.07−0.4 mm we have established that the effect observed is similar to the bulklike one. Because the free carriers are not able to penetrate more than 85 nm, one can expect a crucial role played by electrostricted phonons propagating through the sample.

Changes of sample thickness do not change substantially the features of the TPA, confirming the bulklike origin of the phenomenon with the nanolayer source.

From the performed experimental investigations and calculations of the TPA and from the band structure one can conclude that the principal requirement for the observation of these effects is the presence of the borate groups. However, the presence of the rare earth ions is necessary for the occurrence of effective anharmonic electron−phonon interaction, and it was shown in our previous works devoted to rare-earth-doped borate crystals.[21] From the performed calculations the particular bands should possess flat band energy dispersion in the **k**-space. As a consequence to observe the mentioned nonlinear optical effects it is necessary to have the wide band energy gap crystal with maximally flattered bands in **k**-space. From known band structures for borates such structure can be observed for the germanate and titanate complexes.[22] However this requires one to perform additional experimental investigations.

4. Conclusions

In this paper we show that lanthanum borate crystals may be of interest due to the UV-operated nonlinear absorption,. We performed photoinduced *Z*-scan measurements using an excimer Xe−F laser ($\lambda = 217$ nm) as a source of the photoinducing beam. The illumination created a thin, near-the-surface layer (80−90 nm) in which photoinduced TPA within the bulk volume was observed. The highest values of the TPA β coefficient were achieved for the polarization of the pumping light directed along the second-order optical axis. The obtained values of the TPA coefficients indicate a possibility of using LBC crystals as optically operated limiters over a wide spectral range. The performed quantum chemical simulations and Raman spectra confirm the substantial role played by UV-induced electron−phonon anharmonicity in the observed effects. Their efficiency is at least 3 times higher than that in the case of BiBO crystals.[15]

Acknowledgment. This work was partly supported by the Polish Committee for Scientific Research, Grant Nos. 1 P03B 058 27 and 4 T11B 051 25.

References and Notes

(1) Chen, C.; Wu, Y.; Li, R. *J. Cryst. Growth* **1990**, *99*, 790−798.

(2) Mori, Y.; Kuroda, I.; Sasaki, T.; Nakai, S. *Jpn. J. Appl. Phys.* **1995**, *34*, L296−L298.

(3) Aka, G.; Khan-Harari, A.; Vivien, D.; Benitez, J. M.; Salin, F.; Godard, J. *Eur. J. Solid State Inorg. Chem.* **1996**, *33*, 727−736.

(4) Lukasiewicz, T.; Kityk, I. V.; Makowska-Janusik, M.; Majchrowski, A.; Galazka, Z.; Kaddouri, H.; Mierczyk, Z. *J. Cryst. Growth* **2002**, *237*−*239*, 641−644.

(5) Hellwig, H.; Liebertz, J.; Bohaty, L. *Solid State Commun.* **1999**, *109*, 249−251.

(6) Ghotbi, M.; Ebrahim-Zadeh, M.; Majchrowski, A.; Michalski, E.; Kityk, I. V. *Opt. Lett.* **2004**, *29*, 2530−2532.

(7) Wu, Y.; Liu, J.; Fu, P.; Wang, J.; Guo, F.; Zhao, G.; Qin, J.; Chen, C. *Proc. SPIE*−*Int. Soc. Opt. Eng.* **1998**, *3556*, 8−13.

(8) Wu, Y.; Fu, P.; Zheng, F.; Wan, S.; Guan, X. *Opt. Mater.* **2003**, *23*, 373−375.

(9) Fu, P.; Wang, J.; Guo, H.; Zhang, H.; Xu, Z.; Guo, F.; Wu, Y. *Prog. Cryst. Growth Charact. Mater.* **2000**, *40*, 107−110.

(10) Fu, P.; Jing, F.; Zheng, F.; Wu, Y. *J. Chin. Ceram. Soc.* **2004**, *32*, 245−247.

(11) Wang, G.; Lu, J.; Cui, D.; Xu, Z.; Wu, Y.; Fu, P.; Guan, X.; Chen, C. *Opt. Commun.* **2002**, *209*, 481−484.

(12) Wang, J.; Fu, P.; Wu, Y. *J. Cryst. Growth* **2002**, *235*, 5−7.

(13) Majchrowski, A.; Borowiec, M. T.; Michalski, E. *J. Cryst. Growth* **2004**, *264*, 201−207.

(14) Boyd, R. W. *Nonlinear Optics*; Academic Press: New York, 1992.

(15) Majchrowski, A.; Kisielewski, J.; Michalski, E.; Ozga, K.; Kityk, I. V.; Lukasiewicz, T. *Opt. Commun.* **2005**, *250*, 334−343.

(16) Sheik-Bahae, M.; Said, A. A.; Wei, T. H.; Hagan, D. J.; Van Styrland, E. W. *IEEE. J. Quantum Electron.* **1990**, *QE*−*26*, 760−769.

(17) Liu, X. D.; Guo, S. L.; Wang, H. T.; Hou, L. T. *Opt. Commun.* **2001**, *197*, 431−437.

(18) Chapple, P. B.; Staromlynska, J.; Herman, J. A.; Mckay, T. J.; Mcduff, R. G. *J. Nonlinear Opt. Phys. Mater.* **1997**, *6*, 251−293.

(19) Maeda, A.; Ono, M.; Kishida, H.; Manako, T.; Sawa, A.; Kawasaki, M.; Tokura, Y.; Okamoto, H. *Phys. Rev. B* **2004**, *70*, 125117.

(20) Reshak, A. H.; Auluck, S.; Kityk, I. V.; Majchrowski, A.; Kasprowicz, D.; Drozdowski, M.; Kisielewski, J.; Lukasiewicz, T.; Michalskui, E. *J. Mater. Sci.* **2006**, doi: 10.1007/S10853-006-4487-5.

(21) Majchrowski, A.; Ebothe, J.; Fuks-Janczarek, I.; Makowska-Janusik, M.; Sahraoui, B.; Kityk, I. V. *Opt. Mater.* **2005**, *27*, 675−678.

(22) Kityk, I. V.; Majchrowski, A.; Sahraoui, B. *Opt. Lasers Eng.* **2005**, *43*, 75−83.